

Article

Fatigue Analysis of Nonstationary Random Loadings Measured in an Industrial Vehicle Wheel: Uncertainty of Fatigue Damage

Julian M. E. Marques ^{1,*} , Luigi Solazzi ²  and Denis Benasciutti ^{3,*} 

¹ Department of Mechanics, Biomechanics and Mechatronics, Faculty of Mechanical Engineering, Czech Technical University, Technická 4, 166 36 Prague, Czech Republic

² Department of Industrial and Mechanical Engineering, University of Brescia, Via Branze 38, 25123 Brescia, Italy; luigi.solazzi@unibs.it

³ Department of Engineering, University of Ferrara, Via Saragat 1, 44122 Ferrara, Italy

* Correspondence: julianmarcell.enzweilermarques@fs.cvut.cz (J.M.E.M.); denis.benasciutti@unife.it (D.B.); Tel.: +39-0532-974976 (D.B.)

Abstract: This article presents an application of a method for estimating the inherent statistical variability of the fatigue damage computed in one single nonstationary random time history. The method applies the concept of confidence interval for the damage, which is constructed after the single time history is subdivided into pseudo-stationary segments, with each of them further divided into shorter blocks. As a case study, the method is applied to the strain time histories measured in a wheel of a telescopic handler industrial vehicle. A preliminary screening involving the short-time Fourier transform and the run test is carried out to verify whether the measured time histories are truly nonstationary and fall within the hypotheses of the proposed method. After that, the confidence interval for the unknown expected damage is computed; its upper bound can be used as a safety limit in a structural integrity assessment. The obtained results seem very promising and suggest the possible use of the proposed approach in similar engineering applications.

Keywords: fatigue damage; nonstationary random loadings; run test; short-time Fourier transform



Citation: Marques, J.M.E.; Solazzi, L.; Benasciutti, D. Fatigue Analysis of Nonstationary Random Loadings Measured in an Industrial Vehicle Wheel: Uncertainty of Fatigue Damage. *Metals* **2022**, *12*, 616. <https://doi.org/10.3390/met12040616>

Academic Editors: Mark T. Whittaker, Turan Dirlik and Anders Jarfors

Received: 25 February 2022

Accepted: 30 March 2022

Published: 2 April 2022

Publisher's Note: MDPI stays neutral with regard to jurisdictional claims in published maps and institutional affiliations.



Copyright: © 2022 by the authors. Licensee MDPI, Basel, Switzerland. This article is an open access article distributed under the terms and conditions of the Creative Commons Attribution (CC BY) license (<https://creativecommons.org/licenses/by/4.0/>).

1. Introduction

Wheels in industrial vehicles are critical components, being subjected in service to complex random and nonstationary fatigue loadings. Here, the term ‘random’ indicates the intrinsic aleatory nature of the loading that makes it impossible to exactly predict the loading values. Instead, ‘nonstationary’ specifies that the statistical properties of the random loading (e.g., mean value, root-mean-square value, autocorrelation function) change over time as a consequence, for example, of the different driving conditions, routes (curves, straights, jolts, etc.), or vehicle usage (e.g., speed, operating modes) [1–4].

When considering the design of industrial vehicles from a material viewpoint, a new trend has recently emerged that exploits a lightweight design based on the use of composite materials not only for wheels [5,6] but also for other structural details of the vehicle (e.g., trucks [7,8], earthmoving machines [9], or working platforms [10,11]). This trend in design aims at improving the wheel and vehicle performance, while reducing the overall weight.

In addition to the material choice, a crucial step in the design process remains the structural integrity assessment of critical parts. For wheels of industrial vehicles, the design process usually develops as a synergistic interaction between numerical modeling and in-field experimental testing [12,13]. The outcomes of numerical simulation analyses are, indeed, supported by experimental tests conducted on prototypes or real vehicles subjected to standardized loadings that should be as representative as possible of the actual loadings observed in service.

Within this experimental framework, one of the most complex tasks is the definition of the testing conditions that lead to the most representative loadings. An example of the

complexity of service loadings is that characterizing the wheels of industrial vehicles in industrial sectors such as agricultural, construction, or material-handling. In these sectors, the wheels have to endure heavy loads characterized by different intensities or that are distributed unevenly as a result of the excitation from an uneven ground. The complexity in loading definition further increases if the loading intensity is correlated to the various wheel geometries that often cover a wide range; for example, the nominal wheel load can range from 4 kN up to 250 kN for a wheel size varying from 8'' (203 mm) to 54'' (1371 mm) in diameter and from 3'' to 36'' in width [12].

Accordingly, it becomes quite unlikely for a single validation test to be able to encompass all the loading conditions to which the wheels will be subjected in their service life, or to include all the number of cycles counted in the entire wheel lifetime; this number is on the order of several millions as determined by the number of wheel revolutions.

If interpreted from a statistical point of view, the definition of appropriate testing loadings for experimental validation becomes a matter of the representativeness and sampling variability of the testing loading. When only a single or, at best, a few loading time histories are recorded from tests, reliable conclusions on the service fatigue life of the wheel can only be made on a statistical basis from the knowledge of a small set of fatigue cycles and few damage values. Such few damage values, however, represent only a small fraction of a much larger population of values that might theoretically be obtained from testing a much larger (virtually infinite) set of time histories—a situation clearly not obtainable in practice. The goal is to deduce meaningful statistical conclusions on the wheel reliability and safety solely from the knowledge of such a small sample of time history records and damage values obtained in experiments.

This issue is intimately related to the inherent statistical variability of fatigue damage. More precisely, let $D(T)$ be the fatigue damage of a time history $z(t)$ of time duration T . From a mathematical point of view, damage $D(T)$ is a random variable that follows a certain probability distribution with expected value $E[D(T)]$ and variance σ_D^2 .

Starting from the pioneering works of Bendat [14] and Mark and Crandall [15,16], several methods have been proposed for estimating $E[D(T)]$ and σ_D^2 from the statistical properties of random loading in the time domain or from its power spectral density in the frequency domain. While the early works were restricted to certain classes of random processes (Gaussian linear oscillator) [14–16], more recent methods made the solution include any kind of Gaussian random loading with specific types of power spectral density, e.g., narrow-band, multimodal, or wide-band [17–19]. An extension to narrow-band and non-Gaussian cases has also been proposed recently [20].

A completely different approach, developed in [21], exploited a data-driven analysis of time history records to account for the variability of the random loading by constructing a confidence interval for the expected damage. The approach, first benchmarked with numerical simulations, was further validated against experimental records for a mountain bike under pseudo-stationary conditions [22].

The approaches mentioned so far are, however, restricted to the case of stationary random loadings with time-invariant statistical properties. This stationary condition, as already emphasized, may be too oversimplified for the nonstationary in-service loadings experienced by the wheels of industrial vehicles.

This work, thus, attempts to extend the confidence interval approach mentioned above to the case of nonstationary random loadings. Although the theoretical framework of the method was preliminary devised in [23,24], the goal here is to apply the method to an actual case study, i.e., to the nonstationary time histories recorded from a wheel of a telescopic handler vehicle.

In a preliminary stage, each recorded time history is confirmed to be really nonstationary by the application of, first, the short-time Fourier transform (STFT) and, then, the run test. The outcome of the STFT allows the time history to be divided into stationary or pseudo-stationary segments. On the basis of such subdivision, it is possible to apply, for each state, the usual method valid for stationary loading to compute the confidence

interval for the expected damage. Confidence intervals for different stationary segments are combined to arrive at the confidence interval for the whole nonstationary time history. The obtained results seem very promising and suggest the possible use of the proposed approach in similar engineering applications.

2. Fatigue Damage and Expected Value

Let $z(t)$, $0 \leq t \leq T$ be a nonstationary time history of time duration T , which acts on a component or structural detail. According to the Palmgren–Miner damage accumulation rule, the fatigue damage of $z(t)$ is computed by summing up the damage of all rainflow cycles

$$D(T) = \sum_{i=1}^{N_T} d_i = \sum_{i=1}^{N_T} \frac{S_i^m}{K} \quad (1)$$

where S_i is the stress amplitude of the i -th rainflow cycle, and N_T is the total number of rainflow cycles counted in $z(t)$. Parameter K is the fatigue strength coefficient, and m is the inverse slope of the S–N curve $S^m N = K$ of the component or structural detail. Below, a single-slope S–N curve is used, but the approach presented hereafter allows for any type of S–N curve. Furthermore, to account for the scatter in material fatigue strength, the S–N curve $S^m N = K$ can be thought to represent a characteristic line defined for a prescribed survival probability and confidence [25].

Since $z(t)$ is a random time history, the fatigue cycles counted in $z(t)$ have randomly distributed amplitudes, and their number N_T is also random. As a result, the damage $D(T)$ in Equation (1) has to be regarded as a random variable, being affected by two sources of randomness related to amplitudes S_i and number of cycles N_T . In other words, the random variables, S and N_T , determine an inherent statistical variability of the damage value $D(T)$ when it is computed from a particular time history $z(t)$. For example, damage $D(T)$ is likely not to be equal if it were computed from other time histories, despite being obtained or measured under virtually identical conditions. From a probabilistic point of view, the random variable $D(T)$ follows a certain probability distribution with expected value $E[D(T)]$ and variance σ_D^2 .

As a result, the damage $D(T)$ computed from a single time history $z(t)$ with finite length T is only a sample value that is distributed randomly around $E[D(T)]$; it may be smaller or larger than $E[D(T)]$. If the ratio $\sigma_D / \sqrt{E[D(T)]}$ (coefficient of variation) is large, the values of $D(T)$ may be so scattered around $E[D(T)]$ that a fatigue life estimation based on a single value $D(T)$ becomes rather uncertain [21].

Since the damage $D(T)$ is a random variable following a certain distribution, the expected damage is given by taking the expectation of Equation (1)

$$E[D(T)] = E\left[\sum_{i=1}^{N_T} d_i\right] = E[N_T] \frac{E[S^m]}{K}, \quad (2)$$

where $E[-]$ is the probabilistic expectation, which represents a weighted average over an infinite population of values.

According to this definition of expectation, the expected damage $E[D(T)]$ in Equation (2) is the average over an infinite population of damage values that are computed from an infinite ensemble of time histories; it clearly represents a mathematical abstraction. In engineering applications, conversely, the common situation is that in which only one time history with duration T is obtained from measurements. In this case, $E[D(T)]$ cannot be computed since the infinite ensemble of time histories is unknown.

The problem then becomes that to make statistical conclusions about $E[D(T)]$ solely on the basis of the knowledge of damage $D(T)$. Since this damage is a random variable with expected value $E[D(T)]$, it is not known a priori the closeness of $D(T)$ and $E[D(T)]$. The damage $D(T)$ can be very close to $E[D(T)]$, or it can be significantly far from $E[D(T)]$. A way to address this issue is to use $D(T)$ for constructing a confidence interval for $E[D(T)]$.

In [21], a $100(1 - \beta)\%$ confidence interval to include $E[D(T)]$ was proposed for the case of a stationary time history. The proposed confidence interval was proven to agree with results from simulated [21] and measured stationary loadings, the latter acquired on a mountain bike [22]. Despite these promising results, the proposed approach was only applied to stationary time histories. In situations where the time history is nonstationary, a different procedure is needed to obtain the confidence interval for $E[D(T)]$.

3. Confidence Interval of Damage in a Nonstationary Loading

This section describes how to construct a confidence interval to enclose the expected damage for the case of a nonstationary switching random time history $z(t)$. The term ‘switching’ indicates that $z(t)$ is formed by a sequence of stationary load states. The number of load states needs to be two or more, $N_S \geq 2$, and they can have same or different time durations, $T_{S,i}$, $i = 1, 2, \dots, N_S$. The total time length of $z(t)$ is $T = \sum_{i=1}^{N_S} T_i$.

Note that the different states can appear in any random sequence in $z(t)$ and any number of times (see Figure 1a), i.e., the same state can appear repeatedly several times in the sequence, as often observed in real applications [26]. In this circumstance, the quantity $T_{S,i}$ indicates the *total* time duration of state i in $z(t)$.

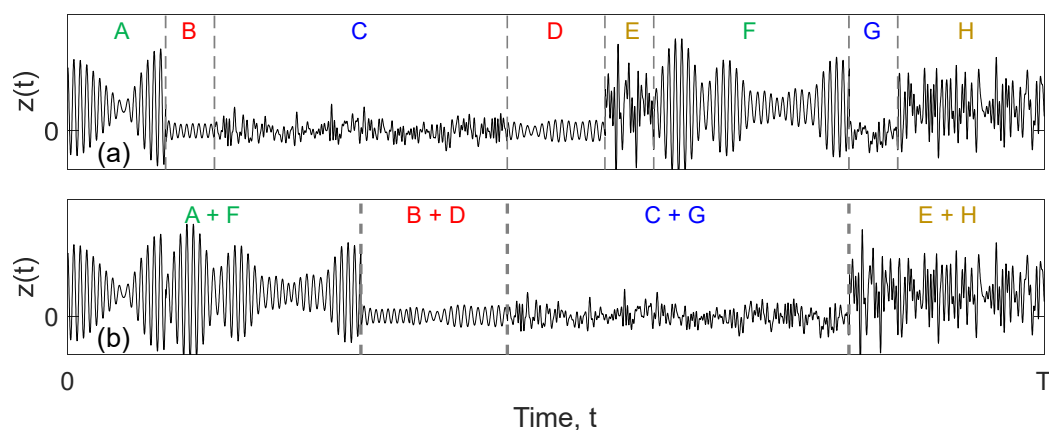


Figure 1. Example of state reordering: (a) nonstationary switching time history with replicated stationary states; (b) the same time history after state reordering.

For the procedure that follows, it is irrelevant in which time order and how many times a stationary state appears in $z(t)$. Hence, in a very first stage, the original sequence of states must be reordered so that, in the sequence, each load state appears only once in its full length $T_{S,i}$. This stage reordering yields a nonstationary time history $z(t)$ without replicated load states (see the example in Figure 1b). While this state reordering will greatly simplify the following analysis, it only causes a small number of cycles to be lost, i.e., those cycles formed by peaks and valleys falling in different states before reordering.

After reordering, the nonstationary time history with load states ordered in sequence is divided into N_S disjoint states of length $T_{S,i}$, $i = 1, 2, \dots, N_S$. A further subdivision of each load state into N_B blocks is then performed; the blocks must be disjoint (not overlapped). Symbol $T_{B,i}$ denotes the time length of blocks in state i . Note that, since each state has in principle a different time length, the use of the same number of block subdivisions for all states makes the blocks in each state have different time lengths.

Within the i -th state, the damage of each block is computed by the rainflow counting method and Palmgren–Miner rule. After subdivision into states and blocks, $N_S \cdot N_B$ damage values $D_{B,ij}(T_{B,i})$, $i = 1, 2, \dots, N_S$ and $j = 1, 2, \dots, N_B$ are obtained, where index i identifies the state and j denotes the block.

Since the states are distinct and the blocks are not overlapped, the damage values $D_{B,ij}(T_{B,i})$ are independent random variables. Furthermore, since each state is stationary,

the damage values $D_{B,ij}(T_{B,i})$, $j = 1, 2, \dots, N_B$ of the blocks within the same i -th stationary state follow the same probability distribution, i.e., they are identically distributed.

A further hypothesis, also adopted in [18,21], is that the block damage values in each state follow a normal probability distribution, which may be different for each stationary state. For the block damage values $D_{B,ij}(T_{B,i})$, the sample mean $\bar{D}_{B,i}(T_{B,i})$ and the sample variance $\hat{\sigma}_{D_{B,i}}^2$ are computed as

$$\begin{aligned}\bar{D}_{B,i}(T_B) &= \frac{1}{N_B} \sum_{j=1}^{N_B} D_{B,ij}(T_{B,i}), \\ \hat{\sigma}_{D_{B,i}}^2 &= \frac{1}{N_B-1} \sum_{j=1}^{N_B} [D_{B,ij}(T_{B,i}) - \bar{D}_{B,i}(T_{B,i})]^2.\end{aligned}\quad (3)$$

The technique of dividing the whole nonstationary time history into stationary states and each state into blocks, and then calculating, for each state, the corresponding sample values of the damage represents a preliminary data processing stage required for the confidence interval of damage to be constructed.

This confidence interval is obtained by reformulating the approximate confidence interval for the difference in means of two independent normal random variables with unknown and unequal variances [27]. Instead of the difference of the means of two variables, the confidence interval here proposed considers the sum in means of two or more random variables. Fortunately, the difference and the sum of normal random variables are also normally distributed.

According to this reformulation, the confidence interval of the expected damage is as follows [23,24]:

$$\begin{aligned}\sum_{i=1}^{N_S} \bar{D}_{B,i}(T_{B,i}) - t_{\beta/2,\nu} \sqrt{\sum_{i=1}^{N_S} \frac{\hat{\sigma}_{D_{B,i}}^2}{N_B}} &\leq \sum_{i=1}^{N_S} E[D_{B,i}(T_{B,i})] \\ &\leq \sum_{i=1}^{N_S} \bar{D}_{B,i}(T_{B,i}) + t_{\beta/2,\nu} \sqrt{\sum_{i=1}^{N_S} \frac{\hat{\sigma}_{D_{B,i}}^2}{N_B}},\end{aligned}\quad (4)$$

in which $t_{\beta/2,\nu}$ is the quantile of Student's t -distribution, and ν is an equivalent number of degrees of freedom

$$\nu \cong (N_B - 1) \frac{\left(\sum_{i=1}^{N_S} \hat{\sigma}_{D_{B,i}}^2\right)^2}{\sum_{i=1}^{N_S} \left(\hat{\sigma}_{D_{B,i}}^2\right)^2}.\quad (5)$$

After substituting the sample mean $\bar{D}_{B,i}(T_{B,i})$ into Equation (4) and multiplying this expression by N_B , the expression of the confidence interval turns out to be

$$\begin{aligned}\sum_{i=1}^{N_S} \sum_{j=1}^{N_B} D_{B,ij}(T_{B,i}) - t_{\beta/2,\nu} \sum_{i=1}^{N_S} \sqrt{N_B \cdot \hat{\sigma}_{D_{B,i}}^2} &\leq \sum_{i=1}^{N_S} N_B E[D_{B,i}(T_{B,i})] \\ &\leq \sum_{i=1}^{N_S} \sum_{j=1}^{N_B} D_{B,ij}(T_{B,i}) + t_{\beta/2,\nu} \sum_{i=1}^{N_S} \sqrt{N_B \cdot \hat{\sigma}_{D_{B,i}}^2}.\end{aligned}\quad (6)$$

Since N_S and N_B can be considered as deterministic values (not random), it is possible to substitute into Equation (6) the single summation of the expected damage of blocks $\sum_{i=1}^{N_S} N_B E[D_{B,i}(T_{B,i})] = E[D(T)]$ and the double summation $\sum_{i=1}^{N_S} \sum_{j=1}^{N_B} D_{B,ij}(T_{B,i}) \cong D(T)$. The double summation well approximates the total damage $D(T)$ since only a small number of cycles are lost after subdivision of the time history into blocks. To ensure that this approximation is acceptable, the number of cycles in each block should be much greater than the number of blocks (see [21]), a condition that is usually met in practice.

After the above mathematical simplifications, the final expression of the $100(1 - \beta)\%$ confidence interval of the expected damage $E[D(T)]$ for a single nonstationary switching time history is

$$D(T) - t_{\beta/2, \nu} \sum_{i=1}^{N_S} \sqrt{N_B \cdot \hat{\sigma}_{D_{B,i}}^2} \leq E[D(T)] \leq D(T) + t_{\beta/2, \nu} \sum_{i=1}^{N_S} \sqrt{N_B \cdot \hat{\sigma}_{D_{B,i}}^2}. \quad (7)$$

This confidence interval can be constructed if a minimum number of blocks $N_B \geq 2$ is available to compute the sample statistics. For $N_S = 1$, Equation (7) yields the result obtained in [21].

In the next sections, this confidence interval is applied to a nonstationary time history measured in a wheel of a telescopic handler vehicle.

4. Experimental Tests

The experimental tests were carried out on the frontal wheel of the loader Manitou MT 1840 (Manitou BF, Ancenis, France) (see Figure 2). The main characteristics of the machine are as follows: weight in unladen conditions 116.3 kN; working load limit on the forks 40 kN; weight in the front axle equal to 54.8 kN in unloaded condition and 129.3 kN with the maximum load on the forks.



Figure 2. Different load conditions applied to the machine: (a) on-road case; (b) load placement case; (c) off-road case; (d) strain gauges and data system applied to the wheel to acquire and register the strain time-histories.

The wheel positioned on the machine is a classical one made of S355 structural steel (UNI EN 10025). The wheel diameter is about 1020 mm, and the width is about 320 mm. On the wheel, a Michelin Power CI 440/80–24" 168 A8 tire (Michelin S.A., Clermont Ferrand, France) was mounted, with an inflate pressure of 4.5 bar. Other details can be found in [12].

As already pointed out, there are many different load conditions that a machine can be subjected to during its life and they depend on several factors such as the route type, velocity, and weight. In the absence of specific standards that help define the load conditions to use for designing the machine and its structural components, four different load cases were analyzed in the experiments. These load conditions were chosen, in agreement with the wheel manufacturer, with the aim to better describe the different uses to which the machine can be subjected during its life.

1. On-road case: the machine moved on a paved road in an oval circuit; this load condition was performed without any load on the forks (Figure 2a);
2. Load placement case: this condition is similar to the previous one except that 20 kN loads at different heights were applied on the loader (Figure 2b);
3. Loader case: in this case, only 40 kN was applied to the machine's forks at a fixed height;
4. Off-road case: the machine moved on an irregular road, with curves and slaloms. The load on the fork was equal to 15 kN, Figure 2c.

Strain gauges (Vishay Precision Group Inc., Raleigh, NC, USA) and an appropriate data logger (Hottinger Bruel & Kjaer, Virum, Denmark) were applied on the wheel to acquire and record the strain signals (see Figure 2d). The strain gauges applied to the wheel were both uniaxial and biaxial (see Figure 3). The grid size was 3 mm, and the resistance was equal to 350 Ω for both strain gauge types. The acquisitions were performed at 100 Hz sampling frequency, a value sufficiently high to avoid missing signal information.

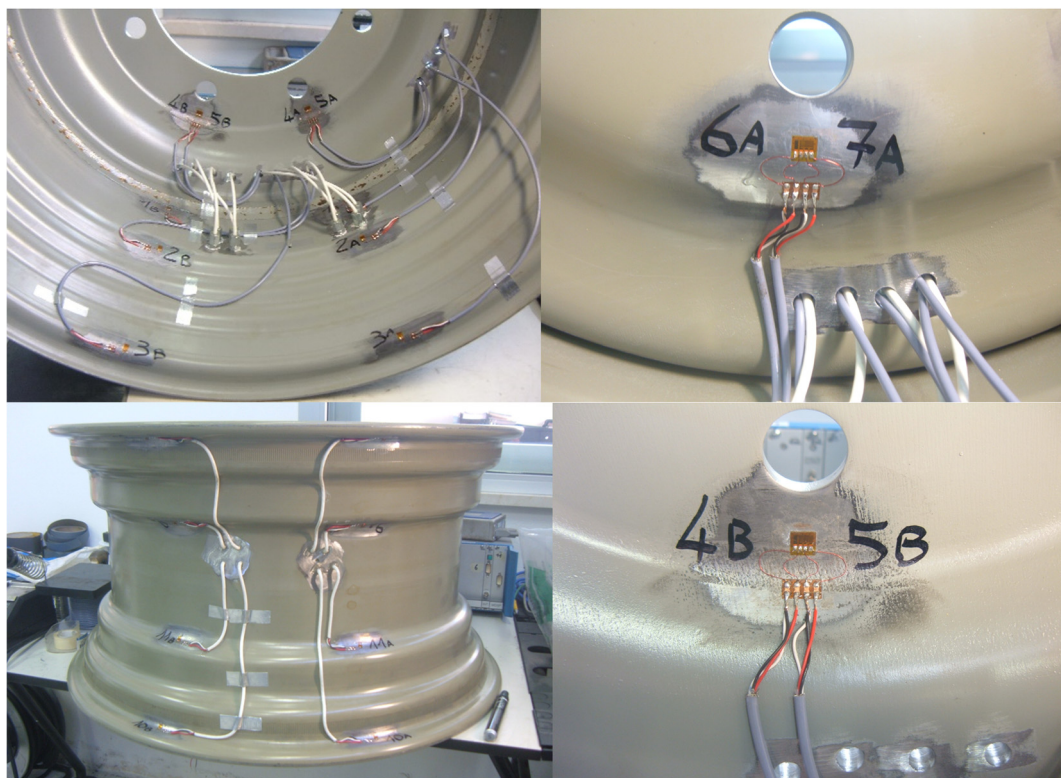


Figure 3. Strain gauges applied to the rim and folder of the wheel.

5. Analysis of the Time History Measured on the Wheel

Among all measured signals, the strain time histories measured on the outer rim of the wheel (strain gauge CH6 in Figure 4) were selected and analyzed in detail with the purpose of illustrating how the confidence interval of damage is constructed. In a preliminary stage, the analysis exploits some signal processing tools that are used to identify and describe some relevant features of the measured time history. Such tools can indicate, both qualitatively and quantitatively, whether the time history is nonstationary.

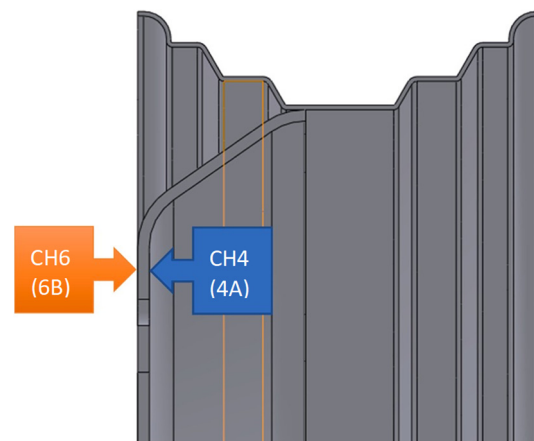


Figure 4. Location of strain gauge for channels CH4 (inner rim) and CH6 (outer rim). Reproduced from [12] with permission from Elsevier.

For the selected strain gauge channel, four time histories, corresponding to the four loading conditions mentioned in Section 4, are available. Each time history represents a well-defined state in which the wheel operates. On the other hand, for the confidence interval method in Section 3 to be applied, the individual time history $z(t)$ needs to be a single nonstationary switching signal formed by different states. For this reason, and for the sake of analysis, the four strain signals from channel CH6 were combined together to form a single nonstationary switching time history $z(t)$ with a total duration of $T = 3456$ s, see Figure 5a.

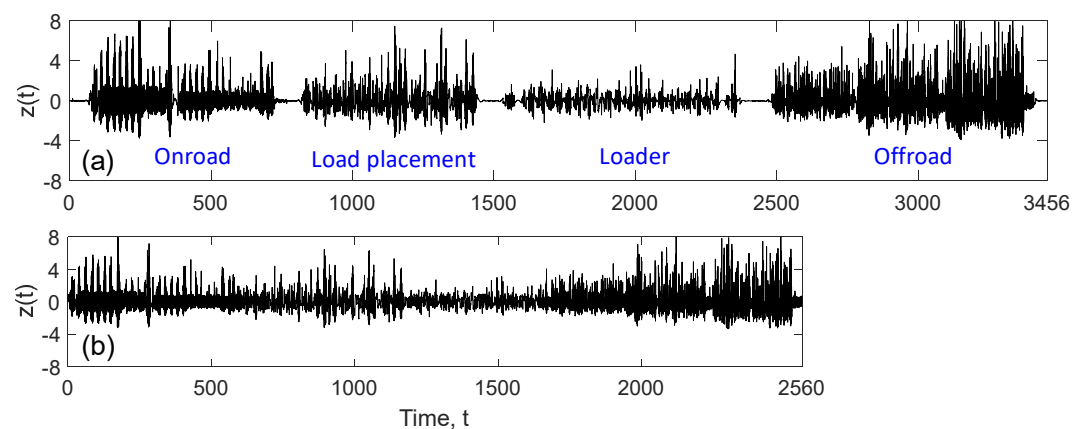


Figure 5. Measured time history used in the analysis (CH6, outer rim): (a) before and (b) after filtering and elimination of steady-state segments.

Nevertheless, this prior information about $z(t)$ was not exploited to decide a priori how many and which stationary states are present in $z(t)$. With the aim of best emphasizing the capabilities of the processing tools in detecting the relevant features of $z(t)$, the analysis proceeded with a sort of “blind approach” in which the only information available was the measured signal $z(t)$ itself.

In a first step, and without loss of generality, the single strain record obtained by measurements was normalized to a signal $z(t)$ with zero mean and unit variance (see Figure 5a). The time history $z(t)$ was very irregular over time t and had a marked nonstationary character.

Figure 5a highlights how the signal was formed by a few segments with zero or practically zero values, corresponding to the vehicle resting in a steady-state condition. These segments were not important for the subsequent analysis since they did not contribute with any fatigue cycle; therefore, they were eliminated by a trigger threshold algorithm

applied directly to the original time history $z(t)$. In addition to this algorithm, a Butterworth filter with a cutoff frequency of 10 Hz was applied to eliminate high-frequency vibrations seen not to be of interest for the subsequent fatigue analysis. In fact, such a cutoff frequency value was higher than the range of frequencies that characterize the vehicle usage in testing and that are related to the low speed of vehicle and to lifting operations. After eliminating the steady-state segments and filtering the original signal, a shorter time history with duration $T = 2560$ s was obtained (see Figure 5b).

The time history $z(t)$ in Figure 5b was processed in the analysis stages described hereafter. It contained the relevant fatigue cycles formed by peaks and valleys, which were obtained by the measurement performed in the vehicle wheel during the duration $T = 3456$ s. As usual in structural durability, the entire time history was subjected to rainflow counting according to the “four-point algorithm” as per the ASTM E 1049 standard [28]; values were discretized into 64 bins. The three-dimensional plot of the rainflow matrix is displayed in Figure 6 as a histogram that shows the statistical distribution of amplitudes and mean values of rainflow cycles.

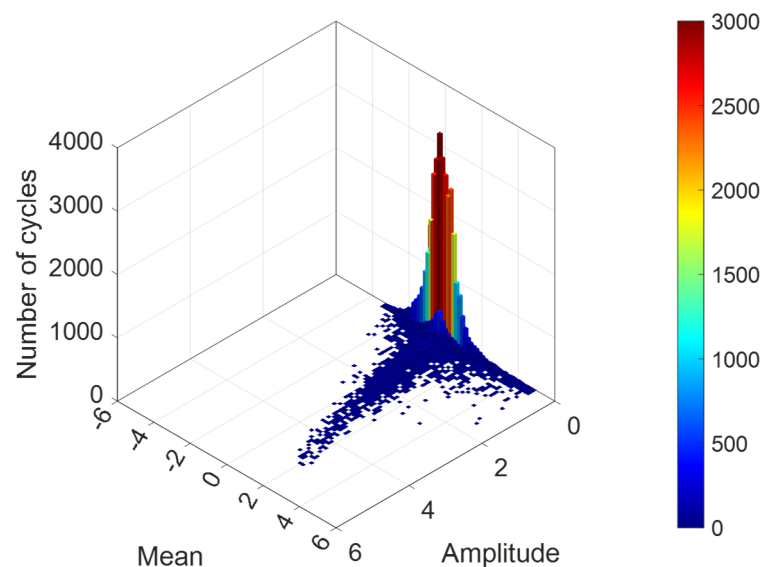


Figure 6. Three-dimensional histogram of rainflow matrix for the measured time history (CH6, outer rim), as a function of normalized amplitude and mean value of counted cycles.

Figure 6 evidences an asymmetric distribution around the zero mean value, with large-amplitude cycles having a positive mean value. Furthermore, Figure 6 demonstrates that the time history had a great deal of low-amplitude cycles with mean zero or close to zero. This trend suggests that the statistical distribution of mean values did not follow a Gaussian distribution, and that of amplitudes did not follow a Rayleigh distribution, as would be expected for a “regular” time history in which cycles have zero mean and symmetrical peak and valley; this type of random signal is often called “narrow-band” in the literature [29].

Although the three-dimensional rainflow matrix is an important characteristic of the signal, it collects in one single ensemble all the fatigue cycles counted in the same measured time history; therefore, it cannot be used to detect whether cycles counted in different portions of the time history follow, in fact, different statistical distributions. As a consequence, the nonstationarity of the measured time history cannot be verified by the rainflow matrix in Figure 6. To this end, other techniques (e.g., level-crossing spectra, cumulative spectra, short-time Fourier transform, run test) are applied to check the nonstationarity of the measured time history. They are grouped into two categories (qualitative and quantitative methods) depending on whether their results allow for conclusions based on statistical methods.

5.1. Qualifying the Nonstationarity

Since the confidence interval in Equation (7) is only applicable to a nonstationary time history formed by a sequence of stationary states, qualitative and quantitative methods were used to verify the nonstationarity of the measured time-history $z(t)$ in Figure 5b.

One qualitative method is based on the comparison of level-crossing spectra computed from different portions into which the whole signal has been divided. The level-crossing spectrum depicts the distribution of the number of times a signal upward crosses (upcrossings) a level [30], as a function of the level. The shape of the crossing spectrum is an indirect measure of the statistical properties of the random signal. The technique used here to check for the presence of a nonstationarity was to divide the time history into segments of equal length and to compare the level-crossing spectrum of each segment.

After dividing the measured time history $z(t)$ into three segments with the same length $T_s = 853.3$ s each, the level-crossing spectrum was computed for each segment; their comparison is illustrated in Figure 7.

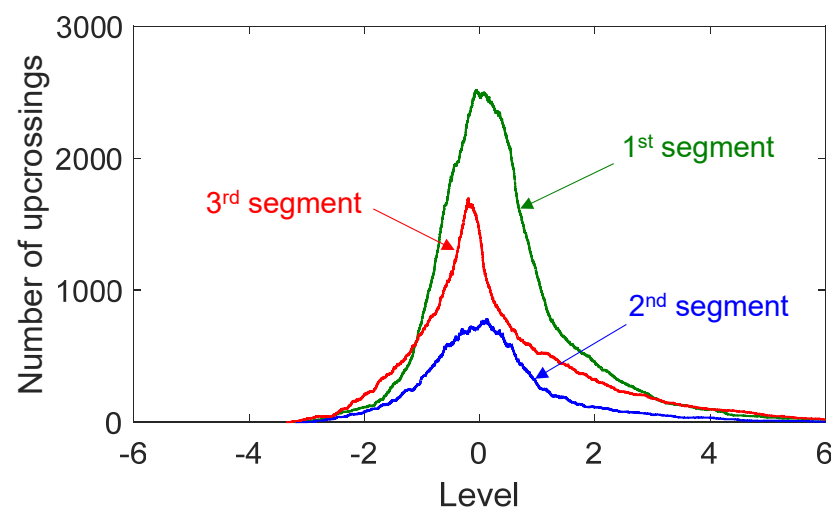


Figure 7. Comparison of level-crossing spectra from three segments of $z(t)$ with duration $T_s = 853.3$ s each (CH6 record, outer rim). Levels are normalized to signal standard deviation.

All three level-crossing spectra were not symmetric; rather, they had a positively skewed distribution characterized by a large number of crossings in the upper tail at positive values, with the presence of crossings even at extreme positive levels. This result is consistent with the presence of cycles with positive mean value observed in the rainflow matrix in Figure 6. In addition, it can be observed that all three level-crossing distributions in Figure 7 showed a similar shape but with a large difference in the number of upcrossings over the levels. This difference is a result in favor of nonstationarity, as it emphasizes the difference in load characteristics from one segment to another.

Another qualitative method to check for nonstationary features is the comparison of the amplitude distribution of rainflow cycles counted in different subsegments of $z(t)$ with same duration. As usual in structural durability, the amplitude distribution is given in terms of a cumulative (or loading) spectrum, which shows how the amplitude varies versus the number of cumulated cycles. The cumulative spectrum is also a useful tool to investigate the cumulative damage behavior [30].

Figure 8 compares three cumulative spectra obtained by first dividing the measured time history $z(t)$ into three segments of same duration $T_s = 853.3$, and then applying the rainflow counting method to each one. The comparison clearly highlights a marked difference in the amplitude distribution. It also reveals that a higher amplitude leads to worse agreement among cumulative spectra. This disagreement further suggests that the measured time history $z(t)$ is nonstationary.

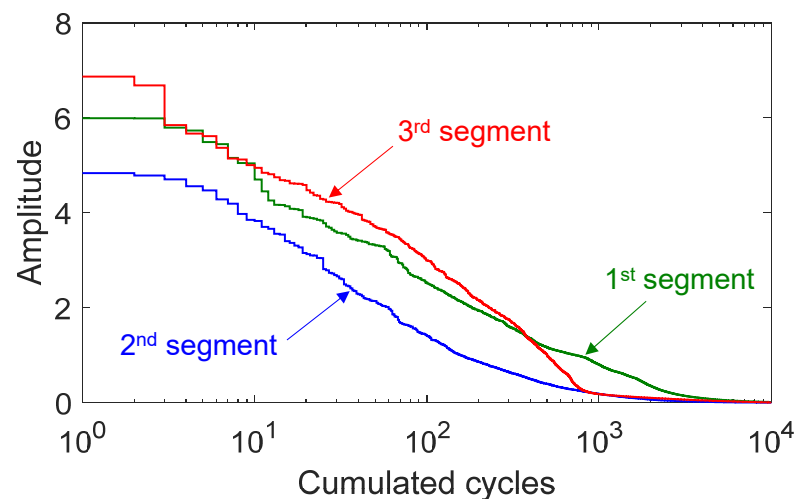


Figure 8. Comparison of cumulative spectra from three segments of $z(t)$ of same duration $T_s = 853.3$ s each (CH6 record, outer rim). Amplitude is normalized to signal standard deviation.

The short-time Fourier transform (STFT) is a method that can be used to analyze how the frequency content of a time history varies over time [31,32]. In order to apply the STFT, the time history must first be divided into a series of short time windows, and the Fourier transform is then computed for the signal within each window.

The method has some requirements to control the resolution achievable in the frequency domain and time domain. The frequency resolution can be improved by increasing the time length of the windows; conversely, the time resolution increases when the window length decreases. These opposite trends (linked to the Heisenberg–Gabor uncertainty principle [33]) emphasize that a high resolution cannot be achieved simultaneously in the time domain and frequency domain; a compromise must be found. On the other hand, taking a time history with fixed time duration T , the STFT plots (spectrograms) in both time and frequency domains are also altered using overlapped windows and zero padding [31]. A positive overlapping between consecutive segments, for example, yields a smoother spectrogram, although it does by no means decrease the estimation error, unlike Welch’s method where overlapping improves the spectrum estimation accuracy [34]. It can indeed be demonstrated that, regardless of segment overlapping, the STFT has a normalized random error (coefficient of variation) of $\sqrt{4/\pi - 1} \cong 0.522$ [32], a value rather large as it means that the standard deviation of the estimate is about one-half of the value being estimated.

Here, the STFT was applied to the measured time history using two different window lengths ($T_w = 10$ s and $T_w = 40$ s) without overlapping and zero padding (see Figure 9). The various colors identify different spectrum levels. A look at the figures shows that, for both window lengths T_w , the frequency content of the signal had significant variations over time t . A marked change in the frequency content is apparent, which in the initial signal portion was mainly concentrated on a narrow range around 2 Hz, before shifting toward lower frequencies and eventually shifting again in the last signal portion to cover a broader frequency range up to 3 Hz. Note that this trend over time can be appreciated best with the spectrogram obtained by a shorter window, which indeed yields a better time resolution. The longer window, by contrast, allows for a better visualization of the frequency content.

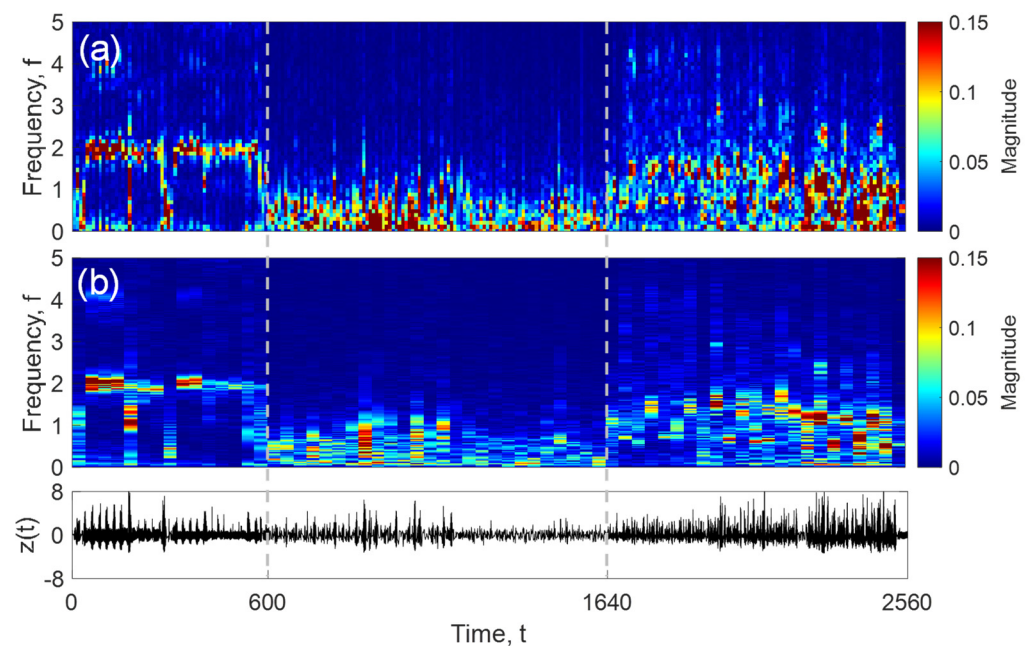


Figure 9. Short-time Fourier transform applied to the measured time history $z(t)$ with two window lengths (CH6 record, outer rim): (a) $T_w = 10$ s and (b) $T_w = 40$ s.

Regardless of window length, a characteristic time evolution clearly emerged. More precisely, Figure 9a,b suggest that the entire signal could approximately be divided into three distinct segments with different frequency content. The first segment can be identified visually from 0 to 600 s, the second from 600 s to 1640 s, and the last from 1640 s to 2560 s. This means that the entire measured time history $z(t)$ could be classified, at least visually, as a nonstationary signal formed by three quasi-stationary or nearly stationary states with different duration T_s . Surprisingly, this finding contrasts with the signal being in fact formed by four portions obtained in four different testing conditions. It may then be concluded that two of the portions had very similar frequency characteristics and could be grouped together for the subsequent derivation of the confidence interval. Albeit apparently contrasting, this result evidences the capabilities of the proposed processing technique for discriminating the various states in $z(t)$ solely on the basis of the knowledge of the signal itself, and without any prior knowledge on the testing conditions, which indeed may often not be available to the analyst.

By considering the outcome of all previous qualitative analyses, the measured time history from the vehicle wheel appears to be nonstationary. This conclusion, albeit quite plausible when also considering the nonstationary testing conditions in which the signal was obtained, was drawn only from a visual inspection of results and, therefore, needs to be supported by further conclusions based on quantitative methods, as considered in the next section.

5.2. Quantifying the Nonstationarity

This section considers a statistical method that can be used to draw conclusions on a quantitative basis on whether the measured time history is nonstationary. The statistical method is a nonparametric test called the Wald–Wolfowitz run test or simply run test [35]. The results obtained from this method are aimed at supporting the conclusions from the more qualitative analysis in the previous section.

The run test can detect whether a sequence of values is characterized by an underlying deterministic (not random) trend that leads to a nonstationary behavior. More specifically, the run test is a hypothesis test that checks for the null hypothesis “the sequence has no deterministic trend and is stationary”. The run test is based on the definition of “run” as a sequence of identical observations followed and preceded by a different observation

or no observation at all [35–37]. The sequence of values is usually classified into two dichotomic categories being above (+) or below (−) a reference value, usually the median of the sequence.

In order to apply the run test to a random time history that is a continuous function of time, a discrete sequence of values must be obtained. For this purpose, the time history is divided into segments and, for each segment, a statistical quantity (usually the root-mean-square (RMS) value) is computed. Accordingly, the time history is converted into a discrete sequence of RMS values, which is then tested for stationarity by the run test [38].

For a sequence with a large number of RMS values (i.e., more than 10), the distribution of runs in the sequence approaches a normal distribution with mean value $\mu_r = E[r]$ and variance $\sigma_r^2 = Var(r)$ [36,37]

$$\mu_r = 1 + n_+, \quad \sigma_r^2 = \frac{n_+(n_+ - 1)}{2n_+ - 1}, \quad (8)$$

where n_+ is the number of observations above the median. Equation (8) assumes that $n_+ = n_-$, i.e., the number of observations above and below the median is equal, a condition that holds true according to the definition of median for an even sequence of values (for an odd sequence, the value equal to the median is discarded, indeed).

In the run test, the acceptance region of the null hypothesis at the significance level β is

$$r_{n_+, 1-\beta/2} < r \leq r_{n_+, \beta/2}, \quad (9)$$

in which $r_{n_+, 1-\beta/2}$ and $r_{n_+, \beta/2}$ are, respectively, the lower and upper limits of the region, which can be found in statistical tables [39] or determined (if the sequence has >10 values) by assuming a normal distribution of runs with μ_r and σ_r^2 in Equation (8).

On the basis of the outcome of the run test, a time history is classified as stationary if the number of runs r falls inside the acceptance region. Otherwise, the time history is classified as nonstationary.

The run test method was here applied to the measured time history $z(t)$ by taking two different values of the segment length ($T_s = 10$ s and $T_s = 20$ s; see Figure 10). The first value coincides with that already used for the STFT. Two different values were considered with the aim of investigating the sensitivity of the run test to the segment length. As already pointed out in [38], a long value of T_s has the effect of smoothing local variations in the RMS value, such that the time history tends to be classified as stationary. Conversely, a too small value of T_s will increase the appearance of the time history as nonstationary [38].

Figure 10a shows the results of the run test when the time segment length was $T_s = 10$ s. For $n_+ = n_- = 128$ observations above and below the median, and a 5% significance level, the upper and lower limits according to Equation (9) are $r_{128, 0.975} = 113.3$ and $r_{128, 0.025} = 144.6$. These limits were obtained by computing the mean and variance in Equation (8) and assuming a normal distribution of runs. The number of runs $r = 83$ was achieved by counting how many times the RMS values, computed in each segment, crossed up and down the median. Given that the observed number of runs $r = 83$ fell outside the acceptance region, the time history was classified as nonstationary by the run test.

The same conclusion was also obtained with a longer segment length (Figure 10b). For the case of $T_s = 20$ s, the number of observations above/below the median was $n_+ = n_- = 64$ and, for a 5% significance, the limits of the acceptance region are now $r_{64, 0.975} = 54$ and $r_{64, 0.025} = 76$. With a longer segment length, the number of runs decreased to $r = 35$, a value that was nevertheless outside the acceptance region for stationarity. Although this value is closer to the lower bound of the region than the previous case, the run test again yielded an indication in favor of nonstationarity.

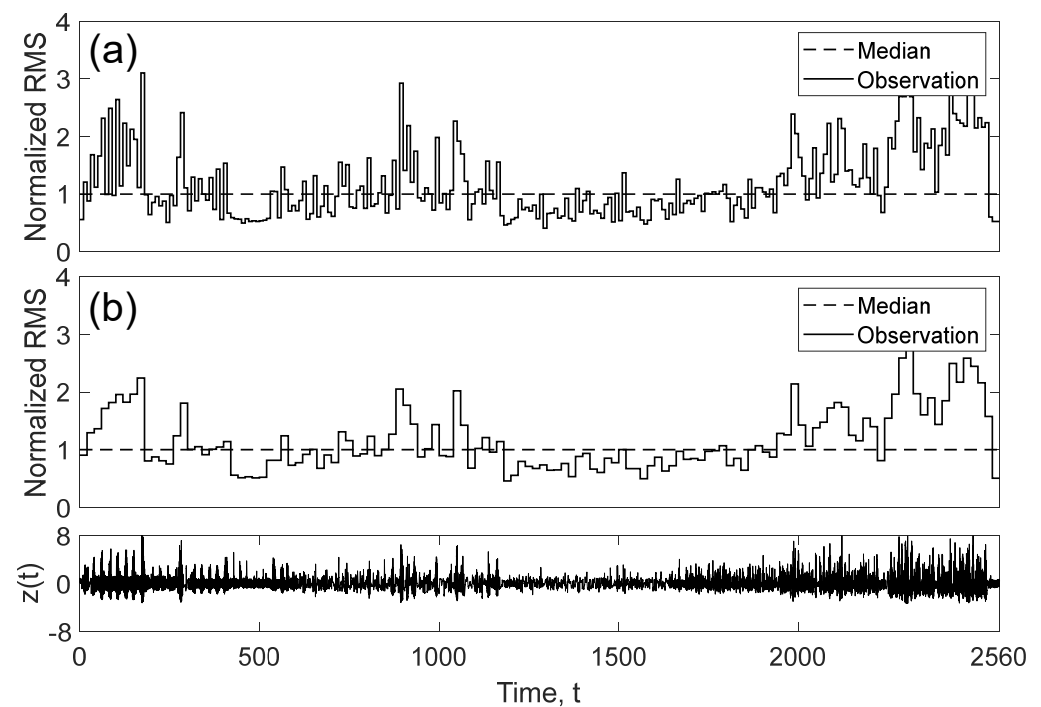


Figure 10. Run test method applied to the measured time history $z(t)$ with two segment lengths (CH6 record, outer rim): (a) $T_s = 10$ s and (b) $T_s = 20$ s.

According to [38], a “stationarity index” $\gamma_r = r/\mu_r$ is defined as the ratio of the observed number of runs to the expected number of runs for a stationary signal. In [38], the parameter γ_r was used as an indicator of the degree of stationarity, where a high value of γ_r indicates that a signal is “more stationary”. For the above examples, the two values would be $\gamma_r = 83/129 = 64.3\%$ (for $T_s = 10$ s) and $\gamma_r = 35/65 = 53.8\%$ (for $T_s = 20$ s), indicating that a shorter segment length made the time history appear as more stationary.

6. Confidence Interval of Damage: Vehicle Wheel Data

After the previous analysis confirmed that the time history $z(t)$ measured in the industrial vehicle wheel (see Figure 5b) is nonstationary and also formed by a sequence of stationary states, it was possible to apply the confidence interval of the damage in Equation (7).

As a first step, the confidence interval required that the individual states in $z(t)$ be identified. On the basis of the results of the STFT analysis, the entire measured signal was divided into three segments ($N_s = 3$). Each segment was identified by the STFT spectrum in Figure 9. These segments may be classified as quasi-stationary or nearly stationary because they have a frequency content almost constant over time.

The confidence interval was constructed with a 95% confidence level by computing the sample values $D_{B,ij}(T_{B,i})$ and $\sigma_{D_{B,ij}}^2$, where $i = 1, 2, 3$ is the number of states and $j = 1, 2, \dots, N_B$ is the number of block subdivisions within each state. $D_{B,ij}(T_{B,i})$ is the fatigue damage in block j located within state i . The damage was calculated by assuming an S-N curve $S^m N = K$ with normalized strength constant $K = 1$ and inverse slope $m = 3$.

The confidence interval was then calculated by varying the number of blocks in the range $N_B = 2, 3 \dots 10$. In the limit case $N_B = 10$, each block contained approximately 600 counted cycles, a number large enough to ensure the approximation of $D(T) \cong \sum_{i=1}^{N_s} \sum_{j=1}^{N_B} D_{B,ij}(T_{B,i})$ to hold, at least for the measured time history $z(t)$ considered in this study. This is confirmed by the results shown below.

Figure 11 displays the confidence intervals of the damage as a function of different number of block subdivisions, N_B . All damage values were normalized to the damage $D(T)$ of the whole time history $z(t)$. The intervals were constructed, according to Equation (7),

around the total damage (solid circles) approximated by the double summation of the sample damage $D(T) \cong \sum_{i=1}^{N_S} \sum_{j=1}^{N_B} D_{B,ij}(T_{B,i})$.

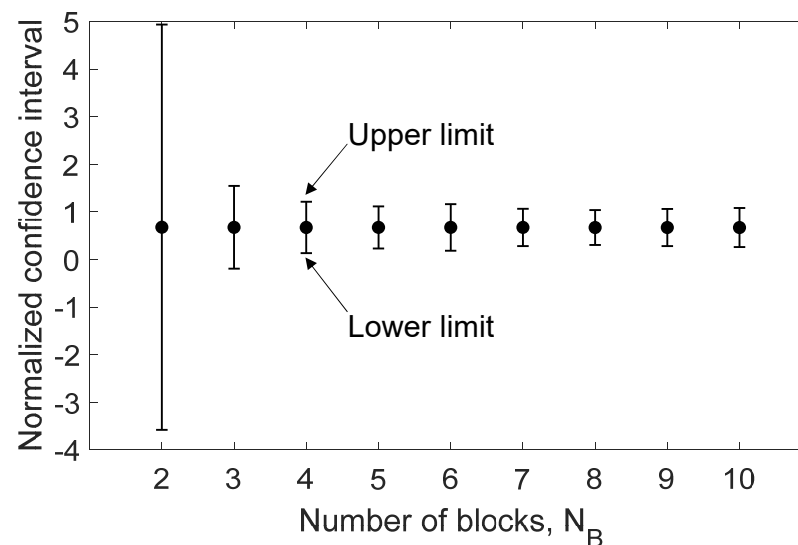


Figure 11. Confidence interval of the damage for the measured time history $z(t)$ from the vehicle wheel (CH6 record, outer rim), as a function of the number of blocks, N_B .

It is interesting to note that the damage value identified by the solid circle remained almost constant for any number of blocks, N_B . This result confirms that the block subdivision eliminated a very negligible number of cycles, such that the approximation $D(T) \cong \sum_{i=1}^{N_S} \sum_{j=1}^{N_B} D_{B,ij}(T_{B,i})$ was perfectly acceptable.

Figure 11 also confirms a general trend already observed in [21] for a stationary time history. The confidence interval became narrower as the number of blocks N_B increased. However, upon increasing N_B , the intervals did not approach zero; rather, they appeared to converge approximately to a sort of minimum interval width.

This outcome means that, while the prediction error for the damage was reduced insofar as the number of block damages (i.e., the block number N_B) increased, it could not become infinitely zero since the number of fatigue cycles was already given in the entire time history. On the other hand, the results shown in Figure 11 prove the importance of using as many blocks as possible in order to decrease the prediction error.

The trends of the confidence intervals here applied to the time history $z(t)$ measured in the industrial vehicle wheel agree with the findings obtained in previous studies with simulations and experiments using mountain bike data [21,22].

Nevertheless, while it was possible for the latter results to be verified by comparison with the expected damage $E[D(T)]$ (which may or may not fall within the confidence interval), this verification was not achievable in the practical case study analyzed here, because the expected damage $E[D(T)]$ was not available.

This circumstance is the rule in practice. Indeed, the expected damage would correspond to the average damage computed over an infinite ensemble of time histories acting on the vehicle wheel, which for obvious reasons was not available. Nevertheless, from the positive feedback from previous validation studies on the same approach presented here, there is reason to believe that the proposed confidence interval approach is in fact correct. On the other hand, in practical applications, it is common to have available only one single measured time history, as in the case study discussed so far in this work.

As a final remark, if the unknown expected damage $E[D(T)]$ were underestimated by the observed value of $D(T)$, a structure or component would be designed unsafely. Only for damage values greater than $E[D(T)]$ would the structure or component be in the safe region. On the other hand, in all such practical cases (as that analyzed in the present

work) in which $E[D(T)]$ is unknown, it is not possible to establish a priori how far $D(T)$ is from $E[D(T)]$. In this regard, the confidence interval, which includes information about the variability of $D(T)$, may help in drawing meaningful conclusions on this point. More specifically, it is suggested to take the upper limit as the reference damage value to be used in design [21].

7. Analysis of Time History from Inner Wheel Rim

In addition to presenting results, the purpose of Section 6 was also to illustrate in great detail the various analysis steps of an individual nonstationary time history. As an example, the procedure was applied to the time history from the outer wheel rim (CH6 in Figure 4). For comparison, the procedure was also applied to the inner rim time history (CH4). Most of the analysis details already discussed in Section 6 are now skipped, thus focusing the attention more on the results.

At first glance, the CH4 time history appears to be very similar to the CH6 record depicted in Figure 5. Upon a closer look, however, it is possible to observe that rainflow cycles were distributed more symmetrically around the global mean value (see Figure 12a). Compared to the distribution in Figure 6, the large-amplitude cycles had a mean value zero or closer to zero. The level-crossing spectra computed in three consecutive segments of the CH4 record are displayed in Figure 12b; they are very similar to those of CH6 shown in Figure 7, apart from the lower number of crossings counted. Interesting in Figure 12b is the peculiar two-spike shape of the level-crossing spectrum in the first segment of the CH4 time history.

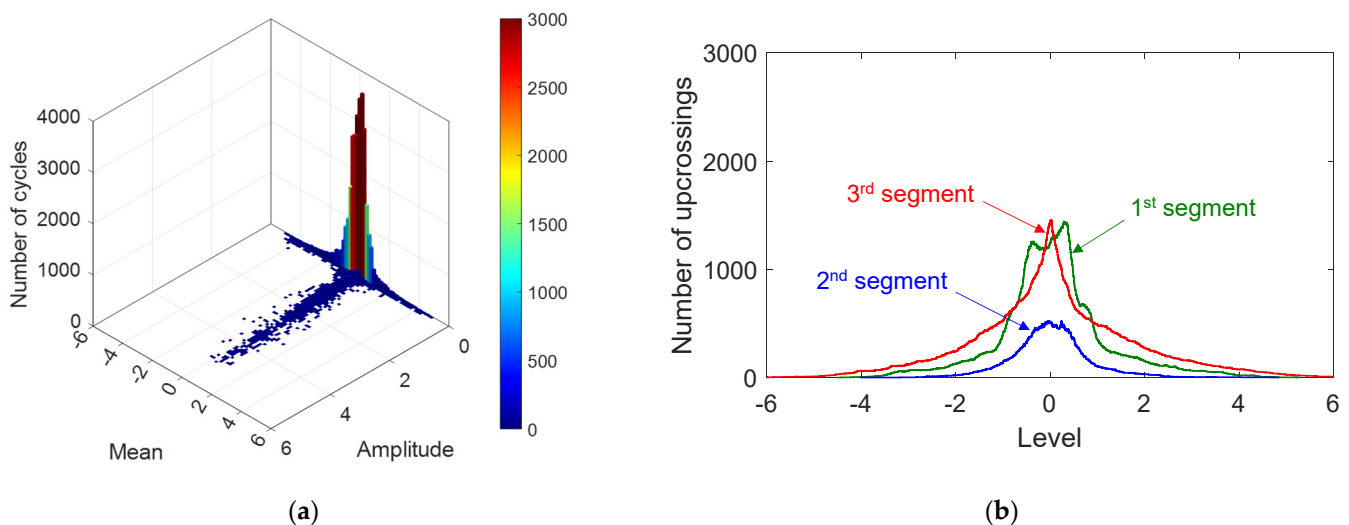


Figure 12. CH4 record, inner rim: (a) Rainflow matrix; (b) level-crossing spectrum. Amplitude, mean and level are normalized to signal standard deviation.

As with the CH6 record, in a preliminary stage, the CH4 time history was also analyzed by the short-time Fourier transform and the run test to detect nonstationary features. As a representative example, Figure 13 shows the results obtained using both techniques when choosing a time window of 10 s. The output for the CH4 time history is practically coincident with that already pointed out for the CH6 signal. Not only did both techniques suggest, visually and quantitatively, that the signal was in fact nonstationary, but they also allowed the signal to be separated for the subsequent analysis into three segments with similar characteristics.

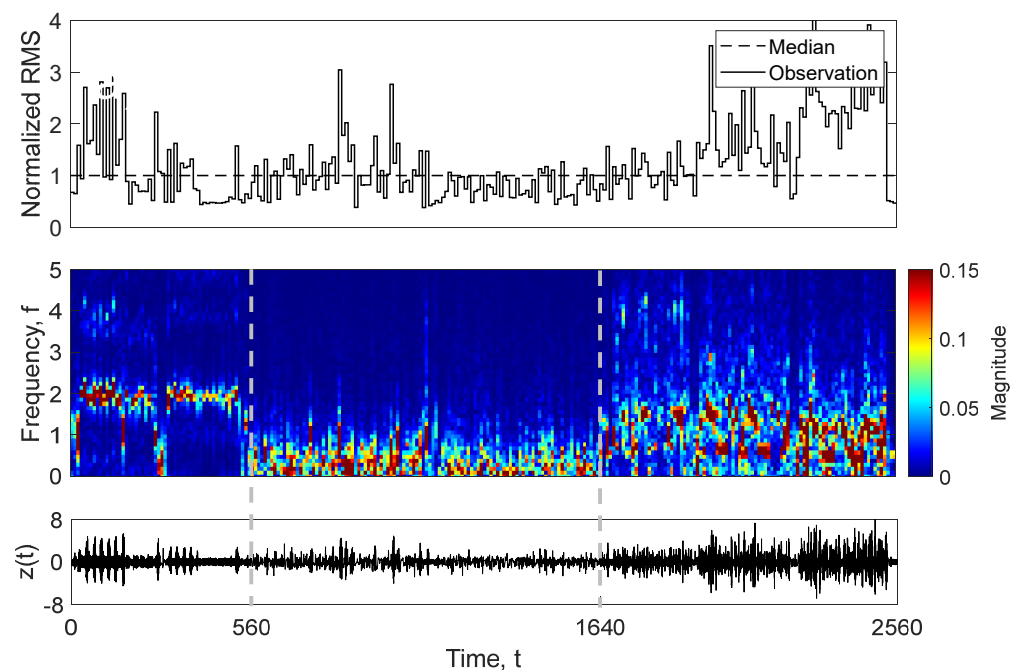


Figure 13. Short-time Fourier transform and run test applied to CH4 time history (inner rim), shown at the bottom of the figure. In both methods, the window time length was 10 s.

Once the individual CH4 time history was divided into three states, and then into blocks, the confidence interval of damage was computed as a function of the number of blocks (see Figure 14). Without a doubt, the results and trends for the CH4 signal are pretty much similar to those obtained for the CH6 time history (see Figure 11).

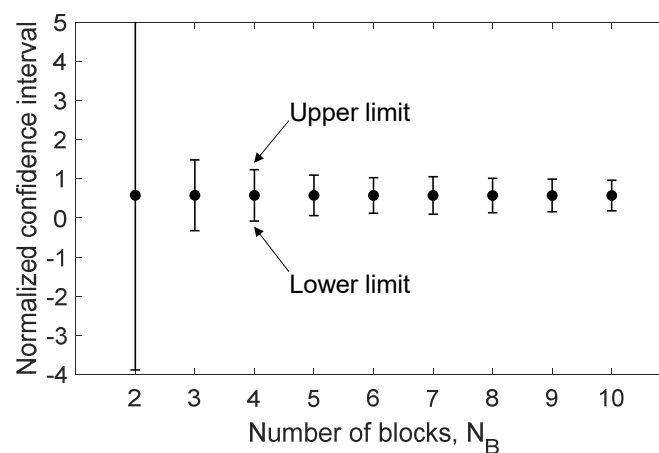


Figure 14. Confidence interval of the damage for the measured time history $z(t)$ from the vehicle wheel (CH4 record, inner rim), as a function of number of blocks, N_B .

8. Conclusions

This article presented an approach for analyzing a single nonstationary random fatigue loading with the purpose of constructing the confidence interval of the expected fatigue damage. Specifically, the approach was applied to a so-called switching nonstationary loading formed by a finite number of stationary or pseudo-stationary states. The obtained confidence interval is a statistical tool to assess the sampling variability of a single fatigue damage value computed from only one individual time history.

The approach was applied here to the strain time histories measured in a wheel of a telescopic handler vehicle when subjected to four testing conditions. The time histories were recorded in the inner and outer wheel rim. In a preliminary phase, qualitative and

quantitative methods (short-time Fourier transform, level-crossing spectrum, run test) were used to deduce some characteristic features of the signal. For example, they allowed deciding how many and which states the whole signal was divided into before calculating the confidence interval. After the loading was divided into states, and each state was further subdivided into smaller portions (blocks), the confidence interval could eventually be determined.

The obtained results allowed reaching the following conclusions:

- The outcomes of both qualitative and quantitative methods suggested that the individual measured signals could in fact be classified as nonstationary. This conclusion was confirmed independently of the choice of the length of the time window used by the short-time Fourier transform (STFT) and by the run test;
- On the basis of the outcome from the STFT, the original single nonstationary time history was divided into three different states. Surprisingly, this finding contrasts with the fact that the signal was, in fact, composed by four consecutive signal portions corresponding to four different loading conditions. It may then be concluded that two of the portions had very similar frequency characteristics and could be grouped together for the subsequent derivation of the confidence interval;
- Subdivision into states and then blocks determined a loss of a very small fraction of fatigue cycles, i.e., those formed by peaks and valleys falling into different states or blocks before subdivision. This small loss by no means affected the accuracy of the calculated confidence interval;
- As the number of blocks increased, the width of the confidence interval decreased, albeit not indefinitely, since it eventually attained approximately a sort of minimum value. This trend confirmed that the prediction error on the expected damage was reduced by increasing the number of blocks, suggesting the use of as many blocks as possible. On the other hand, the fact that the confidence interval width did not approach zero also highlighted that an increase only in the number of blocks would not yield any additional information on the cycle distribution to allow for a further increase in prediction accuracy, i.e., the amount of information was established by the set of fatigue cycles characterizing the given individual time history;
- In conclusion, it is suggested to use the upper limit of the confidence interval of damage as a design value in a structural durability assessment.

Author Contributions: Conceptualization, J.M.E.M. and D.B.; experiments, L.S.; data analysis, J.M.E.M.; writing—original draft preparation, J.M.E.M.; writing—review and editing, D.B. and L.S.; supervision, D.B. All authors have read and agreed to the published version of the manuscript.

Funding: The research activity of one author (J.M.E.M.) was partially funded by the CTU Global Postdoc Fellowship Program (research topic #2-11).

Data Availability Statement: Data are contained within the article.

Acknowledgments: The authors would like to thank Eng. Gianpietro Bramè of Moveero Ltd. company for the information provided during the development of this research.

Conflicts of Interest: The authors declare no conflict of interest.

References

1. Balkwill, J. Weight transfer and wheel loads. In *Performance Vehicle Dynamics: Engineering and Applications*; Elsevier: Amsterdam, The Netherlands, 2018. [\[CrossRef\]](#)
2. Peeters, M.; Kloster, V.; Fedde, T.; Frerichs, L. Integrated wheel load measurement for tractors. *Landtechnik* **2018**, *73*, 116–128. [\[CrossRef\]](#)
3. Muhlmeier, M. Evaluation of wheel load fluctuations. *Int. J. Veh. Des.* **1995**, *16*, 397–411. [\[CrossRef\]](#)
4. Solazzi, L. Wheel rims for industrial vehicles: Comparative experimental analyses. *Int. J. Heavy Veh. Syst.* **2011**, *18*, 214–225. [\[CrossRef\]](#)
5. Xiaoyin, W.; Xiandong, L.; Yingchun, S.; Xiaofei, W.; Wanghao, L.; Yue, P. Lightweight design of automotive wheel made of long glass fiber reinforced thermoplastic. *Proc. Inst. Mech. Eng. Part C J. Mech. Eng. Sci.* **2016**, *230*, 1634–1643. [\[CrossRef\]](#)

6. Wilczynski, A.; Bartczak, M.; Siczek, K.; Kubiak, P. Carbon fibre reinforced wheel for fuel ultra-efficient vehicle. *Mech. Mech. Eng.* **2018**, *22*, 1419–1437. [CrossRef]
7. Solazzi, L. Applied research for weight reduction of an industrial trailer. *FME Trans.* **2012**, *40*, 57–62.
8. Collotta, M.; Solazzi, L. New design concept of a tank made of plastic material for firefighting vehicle. *Int. J. Automot. Mech. Eng.* **2017**, *14*, 4603–4615. [CrossRef]
9. Solazzi, L.; Assi, A.; Ceresoli, F. Excavator arms: Numerical, experimental and new concept design. *Compos. Struct.* **2019**, *217*, 60–74. [CrossRef]
10. Solazzi, L.; Scalmana, R. New design concept for a lifting platform made of composite material. *Appl. Compos. Mater.* **2013**, *20*, 615–626. [CrossRef]
11. Solazzi, L. Experimental and analytical study on elevating working platform. *Procedia Eng.* **2017**, *199*, 2597–2602. [CrossRef]
12. Cima, M.; Solazzi, L. Experimental and analytical study of random fatigue, in time and frequencies domain, on an industrial wheel. *Eng. Fail. Anal.* **2021**, *120*, 105029. [CrossRef]
13. Mazzoni, A.; Solazzi, L. Experimental field test on a multipiece steel wheel and influence of the material properties on its fatigue life evaluation. *Eng. Fail. Anal.* **2022**, *135*, 106106. [CrossRef]
14. Bendat, J.S. Probability Functions for Random Responses: Prediction of Peaks, Fatigue Damage, and Catastrophic Failures. NASA-CR-33, 1 April 1964. Available online: <https://ntrs.nasa.gov/api/citations/19640008076/downloads/19640008076.pdf> (accessed on 31 January 2022).
15. Mark, W.D. The Inherent Variation in Fatigue Damage Resulting from Random Vibration. Ph.D. Thesis, Department of Mechanical Engineering, Massachusetts Institute of Technology (M.I.T), Cambridge, MA, USA, 1961.
16. Crandall, S.H.; Mark, W.D.; Khabbaz, G.R. The variance in Palmgren-Miner damage due to random vibration. In Proceedings of the 4th US National Congress of Applied Mechanics, Berkeley, CA, USA, 18–21 June 1962; Rosenberg, R.M., Ed.; American Society of Mechanical Engineers (ASME): New York, NY, USA, 1962; Volume 1, pp. 119–126.
17. Madsen, H.O.; Krenk, S.; Lind, N.C. *Methods of Structural Safety*; Prentice-Hall: Hoboken, NJ, USA, 1986.
18. Low, Y.M. Variance of the fatigue damage due to a Gaussian narrowband process. *Struct. Saf.* **2012**, *34*, 381–389. [CrossRef]
19. Low, Y.M. Uncertainty of the fatigue damage arising from a stochastic process with multiple frequency modes. *Probab. Eng. Mech.* **2014**, *36*, 8–18. [CrossRef]
20. Marques, J.M.E.; Benasciutti, D. Variance of the fatigue damage in non-Gaussian stochastic processes with narrow-band power spectrum. *Struct. Saf.* **2021**, *93*, 102131. [CrossRef]
21. Marques, J.M.E.; Benasciutti, D.; Tovo, R. Variability of the fatigue damage due to the randomness of a stationary vibration load. *Int. J. Fatigue* **2020**, *141*, 105891. [CrossRef]
22. Marques, J.M.E. Confidence intervals for the expected damage in random loadings: Application to measured time-history records from a Mountain-bike. *IOP Conf. Ser. Mater. Sci. Eng.* **2021**, *1038*, 012025. [CrossRef]
23. Marques, J.M.E.; Benasciutti, D. Evaluating confidence interval of fatigue damage from one single measured non-stationary time-history. In Proceedings of the VIRTUAL 20th International Colloquium on Mechanical Fatigue of Metals, Wrocław, Poland, 15–17 September 2021.
24. Benasciutti, D.; Marques, J.M.E. Methods for estimating the statistical variability of the fatigue damage computed in one single stationary or non-stationary random time-history record. In Proceedings of the 3rd International Conference on Structural Integrity for Offshore Energy Industry (STRUCTURAL INTEGRITY—2021), Aberdeen, UK, 15–16 November 2021; ASRANet Ltd.: Glasgow, UK, 2021; pp. 28–37, ISBN 978-1-8383226-3-2.
25. ASTM E739–10 (2015); Standard Practice for Statistical Analysis of Linear or Linearized Stress-Life (S-N) and Strain-Life (ϵ -N) Fatigue Data. ASTM International: West Conshohocken, PA, USA, 2017. Available online: <https://www.astm.org/e0739-10r15.html> (accessed on 10 February 2022).
26. Johannesson, P. Rainflow cycles for switching processes with Markov structure. *Probab. Eng. Inform. Sci.* **1998**, *12*, 143–175. [CrossRef]
27. Montgomery, D.C.; Runger, G.C. *Applied Statistics and Probability for Engineers*, 6th ed.; John Wiley & Sons: Hoboken, NJ, USA, 2014.
28. ASTM E1049–85; Standard Practices for Cycle Counting in Fatigue Analysis. ASTM International: West Conshohocken, PA, USA, 2017. Available online: <https://www.astm.org/e1049-85r17.html> (accessed on 10 February 2022).
29. Benasciutti, D. *Fatigue Analysis of Random Loadings: A Frequency Domain Approach*; LAP Lambert Academic Publishing: Saarbrücken, Germany, 2012; ISBN 9783659123702.
30. Johannesson, P.; Speckert, M. *Guide to Load Analysis for Durability in Vehicle Engineering*; John Wiley & Sons: Hoboken, NJ, USA, 2014.
31. Cohen, L. *Time-Frequency Analysis*; Prentice-Hall: Hoboken, NJ, USA, 1995.
32. Bendat, J.S.; Piersol, A.G. *Random Data: Analysis and Measurement Procedures*, 4th ed.; John Wiley & Sons: Hoboken, NJ, USA, 2010.
33. Mallat, S. *A Wavelet Tour of Signal Processing: The Sparse Way*, 3rd ed.; Academic Press: Cambridge, MA, USA, 2009.
34. Welch, P.D. The use of Fast Fourier Transform for the estimation of power spectra: A method based on time averaging over short, modified periodograms. *IEEE Trans. Audio Electroacoust.* **1967**, *15*, 70–73. [CrossRef]
35. Wald, A.; Wolfowitz, J. On a test whether two samples are from the same population. *Ann. Math. Stat.* **1940**, *11*, 147–162. [CrossRef]

-
36. Hald, A. *Statistical Theory with Engineering Applications*; John Wiley & Sons: Hoboken, NJ, USA, 1955.
 37. Mood, A.M. The distribution theory of runs. *Ann. Math. Stat.* **1940**, *11*, 367–392. [[CrossRef](#)]
 38. Rouillard, V. Quantifying the non-stationarity of vehicle vibrations with the run test. *Packag. Technol. Sci.* **2014**, *27*, 203–219. [[CrossRef](#)]
 39. Swed, F.S.; Eisenhart, C. Tables for testing randomness of grouping in a sequence of alternatives. *Ann. Math. Stat.* **1943**, *14*, 66–87. [[CrossRef](#)]